THE JOURNAL OF PHYSICAL CHEMISTRY A

 VOLUME 106, NUMBER 37, SEPTEMBER 19, 2002

LETTERS

Periodic-Orbit Analysis of Coherent Electron-Transfer Femtosecond Experiments

Stefan Dilthey and Gerhard Stock*

Institute of Physical and Theoretical Chemistry, J. W. Goethe University, Marie-Curie-Str. 11, D-60439 Frankfurt, Germany

Received: April 8, 2002; In Final Form: July 12, 2002

Femtosecond time-resolved experiments on chemical and biophysical electron-transfer systems may reveal complicated coherent beating which often cannot be simply attributed to nuclear motion on a single Born−Oppenheimer potential-energy surface but rather reflects electronic transitions driven by coherent nuclear motion. To facilitate an intuitive classical interpretation of these experiments, a recently proposed theoretical formulation is employed that affords an exact mapping of discrete electronic states onto continuous degrees of freedom and therefore provides a well-defined classical limit of a nonadiabatically coupled system. The formulation is used to consider the classical periodic orbits of an electron-transfer system, i.e., trajectories that describe periodic nuclear motion on several coupled potential-energy surfaces. Employing concepts of semiclassical periodic-orbit theory, it is demonstrated that transient oscillations observed in electron-transfer femtosecond experiments may be explained in terms of a few classical trajectories.

With the advent of femtosecond laser pulses it has become possible to observe the nuclear motion during a chemical reaction in real time.[1] This is achieved by a pump−probe type experiment in which the molecular system is prepared at time $t = 0$ by a first laser pulse (the "pump") into a nonstationary state, whose time evolution is interrogated by a second laser pulse (the "probe") at the delay time Δt. Employing ultrashort laser pulses, the transient absorption of a polyatomic system may exhibit multiple kinetics and complex oscillation patterns, thus reflecting coherent wave packet motion on multidimensional potential-energy surfaces.

In many cases, however, the interpretation of photoinduced molecular dynamics is complicated by the fact that the underlying Born−Oppenheimer assumption of noninteracting adiabatic potential-energy surfaces may break down. This becomes evident, for example, for molecules exhibiting internal conversion or photoinduced electron transfer.[2] Here, various groups have reported transient spectra showing complicated oscillations, which often cannot be simply attributed to nuclear motion on a single Born−Oppenheimer potential-energy surface but rather reflect electronic transitions driven by coherent nuclear motion.[3]

To facilitate a classical interpretation of these nonadiabatic processes, we have recently proposed a bosonization formulation that affords a well-defined classical limit of a vibronically coupled system.[5] Moreover, the approach allows us to introduce the classical periodic orbits of a vibronic system.[6] Periodic orbits, i.e., solutions of the classical equation of motion that return to their initial conditions, are of particular interest, because they can be directly linked to spectral response functions via semiclassical trace formulas.[7] In favorable cases, periodic-orbit theory allows us to interpret complex absorption spectra in terms of only a few classical trajectories.[8] Considering the vibronic periodic orbits of a simple electron-transfer model, it is the goal of this work to obtain a clear and physically appealing interpretation of femtosecond experiments reflecting coherent electron-transfer.

* Corresponding author. E-mail: stock@theochem.uni-frankfurt.de

10.1021/jp0209188 CCC: $22.00
Published on Web 08/24/2002

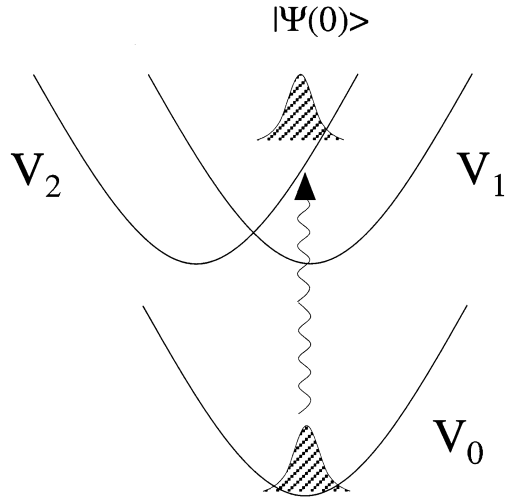

Figure 1. Schematic representation of the potential-energy curves of the electron-transfer model. Following impulsive laser excitation from the electronic ground-state potential V_0, the system exhibits coherent wave packet motion on the nonadiabatically coupled potentials V_1 and V_2.

As a simple example, let us consider a standard model of electron transfer (ET) with the Hamiltonian[9]

$$H = \sum_{n,m} |\psi_n\rangle h_{nm} \langle\psi_m|$$

$$h_{nn} = E_n + \frac{1}{2}\omega(x^2 + p^2) + \kappa_n x \qquad (1)$$

It describes an electronic coupled two-state system ($n, m = 1, 2$), comprising the vibrational Hamiltonian $h_{nn} = T + V_n$ in the electronic state $|\psi_n\rangle$ as well as the off-diagonal coupling elements $h_{12} = h_{21} = g$, which are assumed to be constant. For simplicity, we restrict ourselves to a harmonic system with a single vibrational mode, where x and p denote the dimensionless position and momentum of the vibrational mode, respectively, ω is its vibrational frequency, κ_n denotes the linear coordinate shift in the electronic state $|\psi_n\rangle$, and we have set $\hbar \equiv 1$.[10] Assuming that the system is initially prepared in state $|\psi_2\rangle$ via impulsive laser excitation from the electronic ground state $|\psi_0\rangle$, the model describes the situation of photoinduced ET promoted by a high-frequency vibrational mode (see Figure 1).

To illustrate the motion of the laser-induced wave packet on the coupled potential-energy curves V_1 and V_2, we consider the time-dependent ET probability distribution

$$P_2(x, t) = \langle\Psi(t)|\hat{P}_2(x)|\Psi(t)\rangle \qquad (2)$$

where $\hat{P}_2(x) = |x\rangle\langle x| \, |\psi_2\rangle\langle\psi_2|$ projects the time-dependent state vector $|\Psi(t)\rangle$ on the nuclear coordinate x and the electronic state $|\psi_2\rangle$. Figure 2A shows a contour plot of the quantum-mechanical time evolution of $P_2(x, t)$, calculated by standard methods.[2] As a consequence of the impulsive $|\psi_0\rangle \rightarrow |\psi_2\rangle$ excitation, the wave function at time $t = 0$ is a Gaussian centered at $x_0 = 3$.[10] With increasing time, the wave packet is seen to undergo an oscillation along x with a period of $\approx$80 fs, which roughly corresponds to the vibrational frequency ω of the model. Since $\int P_2(x, t)\, dx$ represents the population probability of the initially excited electronic state $|\psi_2\rangle$, the color-coded intensity pattern also monitors the ET dynamics of the system. In particular, it is seen that the nuclear motion is directly linked to an oscillation of the electronic population, i.e., the vibrational dynamics triggers electronic transitions between the two coupled states $|\psi_1\rangle$ and $|\psi_2\rangle$. A closer analysis of Figure 2A reveals that this simple model of ET already gives rise to a wealth of coherent features. These features reflect nuclear (not electronic) coherence, as $P_2(x, t)$ describes the electronic population. In addition to a general dispersion of the wave packet due to the nonadiabatic transitions, one can observe double-peak structures of the main recurrences of the electronic population as well as the occurrence of various side maxima.

To study to what extent these structures can be monitored in a femtosecond experiment, we now assume that the wave packet dynamics is probed at time $t = \Delta t$ by a second laser pulse $E_P(t)$ that causes stimulated emission from the optically bright state $|\psi_2\rangle$ back to the electronic ground state $|\psi_0\rangle$.[10,11] Employing the time-dependent perturbation theory with respect to the field-matter interaction $H_{int} = -\hat{\mu}E_P(t)$, the transient stimulated-emission spectrum can be written as[2,12]

$$I(\omega_P, \Delta t) = \langle\Psi_P(t)|\Psi_P(t)\rangle$$

$$|\Psi_P(t)\rangle = i\int_{-\infty}^{\infty} dt' E_P(t')\, e^{-iH(t-t')}\hat{\mu}|\Psi(t')\rangle \qquad (3)$$

where ω_P denotes the carrier frequency of the probe field $E_P(t)$. Evaluating eq 3 for Gaussian laser pulses with a duration of 10 fs (panel A) and 20 fs (panel B), Figure 3 shows the femtosecond pump−probe spectra obtained for the ET model. Apart from the pulse-induced averaging in frequency and time, the time evolution of the spectrum is seen to match the nonadiabatic wave packet dynamics shown in Figure 2A in almost every detail, thus highlighting the promise of "femtochemistry" to monitor elementary molecular processes in real time.[1]

While the quantum-mechanical computation of ET dynamics and spectra is straightforward, it is not that clear how to achieve a classical description of nonadiabatic transitions, because discrete electronic states do not possess an obvious classical analogue. As a remedy, various mixed quantum-classical formulations such as the "surface-hopping" model and the "Ehrenfest mean-field" ansatz have been suggested.[13] Because electronic and nuclear degrees of freedom are treated on a different dynamical footing, however, these theories do not necessarily provide a satisfying classical picture of nonadiabatic dynamics.

As an alternative approach to incorporate quantum degrees of freedom in a classical formulation, it has recently been proposed to utilize quantum-mechanical bosonization techniques, i.e., to represent discrete electronic states by continuous harmonic oscillators, which possess a well-defined classical limit.[5] This is achieved by the mapping relations

$$|\psi_n\rangle\langle\psi_m| \rightarrow \frac{1}{2}(X_n X_m + P_n P_m - \delta_{nm}) \qquad (4)$$

$$|\psi_n\rangle \rightarrow |0_1, ..., 1_n, ..., 0_N\rangle \qquad (5)$$

where X_n, P_n are position and momentum operators of the nth oscillator with commutation relations $[X_n, P_m] = i\delta_{nm}$, and $|0_1, ..., 1_n, ..., 0_N\rangle$ denotes a harmonic-oscillator eigenstate with a single quantum excitation in the mode n.[14] Inserting eq 4 into eq 1, we obtain the boson representation of the ET system

$$H = \frac{1}{2}\sum_{n,m} h_{nm}(X_n X_m + P_n P_m - \delta_{nm}) \qquad (6)$$

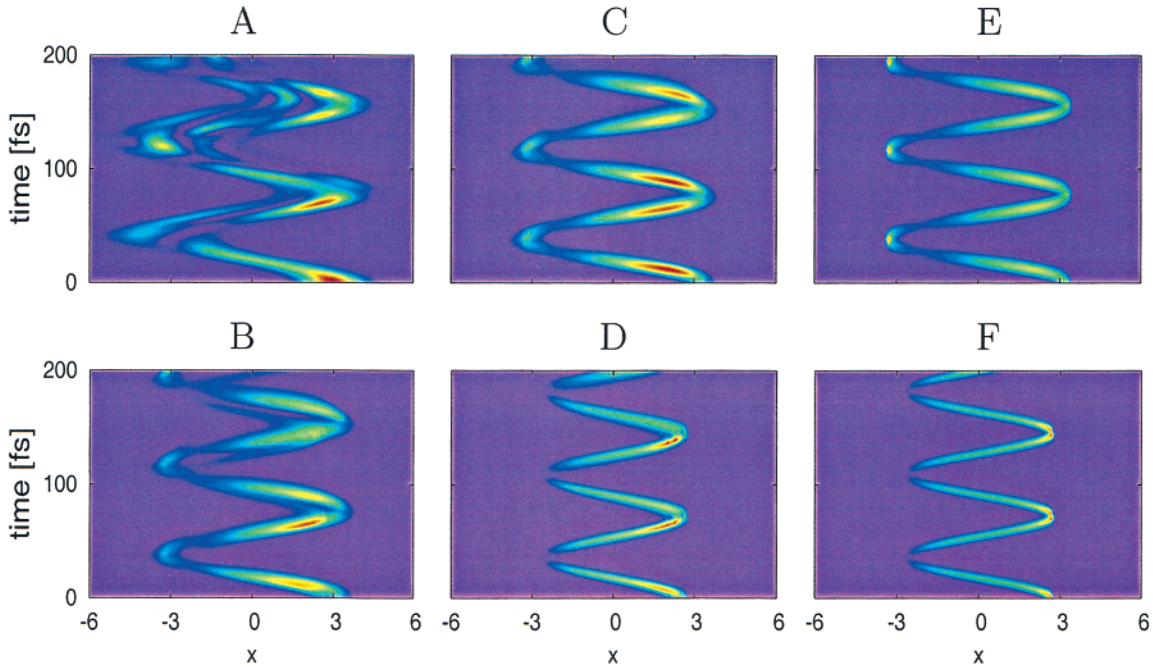

Figure 2. Time evolution of the electron-transfer probability distribution $P_2(x, t)$. The rainbow-color-coded intensity oscillations reflect electronic transitions driven by coherent nuclear motion along the coordinate x. Compared are exact quantum (A) and approximate classical (B) results. The latter are composed of the contributions of the two shortest periodic orbits of the system, which are shown with (C, D) and without (E, F) energy averaging of the orbits.

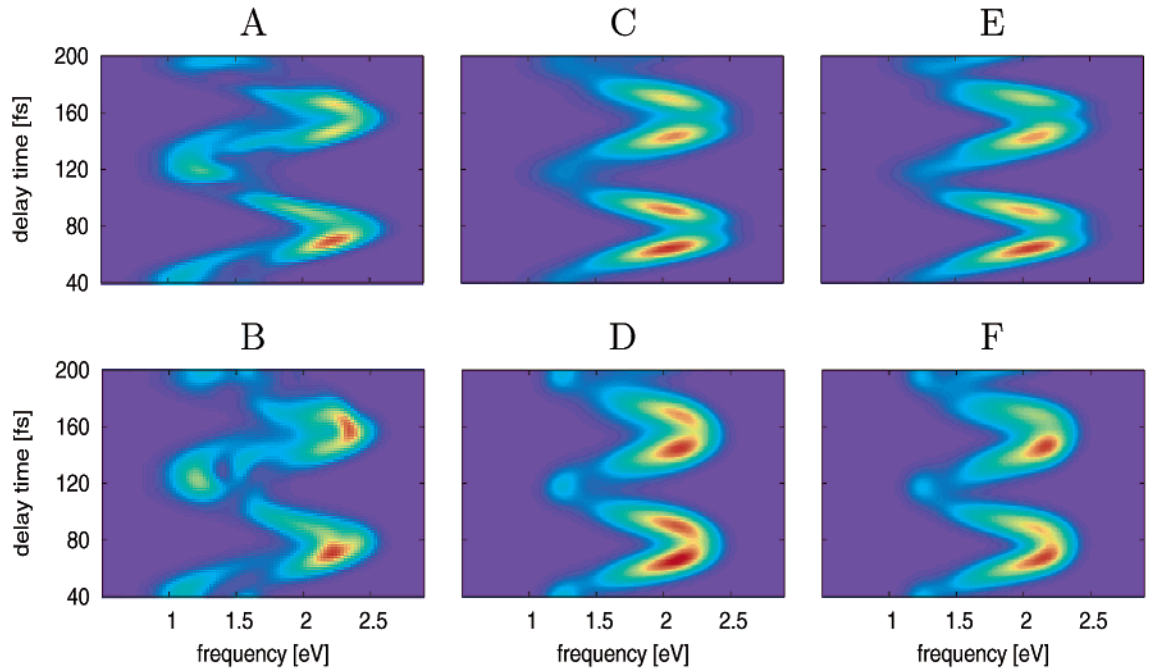

Figure 3. Time- and frequency-resolved stimulated-emission spectra of the coherent electron-transfer process, assuming probe pulse durations of 10 fs (upper panels) and 20 fs (lower panels). Compared are exact quantum data (A,B) and classical periodic-orbit results, which are obtained with (C,D) and without (E,F) energy averaging of the orbits. To avoid confusion arising from overlapping pump and probe laser fields, the signal is shown only for delay times ≥ 40 fs.

As the mapping Hamiltonian (eq 6) contains only continuous operators, the quantum-mechanical system has a well-defined classical analogue. The transition to classical mechanics is performed by changing from the Heisenberg *operators* $y_k(t)$ ($y_k = X_n, P_n, x, p$) obeying Heisenberg's equations of motion ($i\dot{y}_k = [y_k, H]$) to the corresponding classical *functions* obeying Hamilton's equations (e.g., $\dot{X}_k = \partial H/\partial P_k$). In this classical limit, the formalism can be shown to recover the classical electron analogue model of Meyer and Miller.[15] Since the mapping formulation is quantum-mechanically exact, it allows us, without any further approximations, to extend well-established classical concepts and techniques to problems of nonadiabatic quantum dynamics.

In addition to numerical studies,[5,16] the mapping formulation also enables us to introduce and study the periodic orbits of the ET system (eq 1). To this end, it is advantageous to eliminate

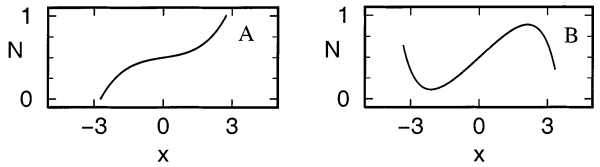

Figure 4. Shortest vibronic periodic orbits of the electron-transfer system, drawn as a function of the nuclear position x and the electronic population N.

one electronic degree of freedom by noting that the total electronic population is conserved.[17] This yields the classical ET Hamiltonian

$$H = \frac{\omega}{2}(x^2 + p^2) + \kappa x(X^2 + P^2 - 2) + gX\sqrt{4 - X^2 - P^2} \tag{7}$$

which consists of a nuclear oscillator (x, p) that is nonlinearly coupled to an electronic oscillator (X, P) representing the two-state system. Analyzing the classical phase−space dynamics of the Hamiltonian (eq 7) under various conditions, the system is found to exhibit mixed classical dynamics: Most of the area of the energetically available phase space belongs to chaotic motion, but there are also some integrable islands which contain fixed points associated with the periodic orbits of the ET system.[6]

To represent the periodic orbits (POs) for a vibronically coupled system in an intuitively clear way, we introduce the classical electronic population variable $N = (X^2 + P^2)/4$, which by construction varies between 0 (system is in $|\psi_1\rangle$) and 1 (system is in $|\psi_2\rangle$). Describing, moreover, the nuclear motion through the position x, Figure 4 shows the two shortest and most important vibronic POs of the ET system. Both orbits shown are self-retracing and reflect the symmetry of the potentials with respect to the $x = 0$ axis. The shortest PO, orbit A, is seen to vibrate between two turning points at $x \approx \pm 2.75$. At the same time, the PO oscillates between the electronic states $|\psi_1\rangle$ and $|\psi_2\rangle$ with a period of 72.8 fs. While orbit A is particularly simple as the vibrational and electronic oscillation occur with the same period, the situation is already somewhat more complicated for orbit B. Within one vibrational cycle taking ≈78.4 fs, this orbit oscillates about three times between the electronic states. It turns out that orbits of type B are of particular importance, because there are numerous POs that are composed of such orbits with slightly shifted turning points.[6]

To express the quantum observables discussed above in terms of the POs of the ET system, we consider the function

$$N_k(x, t) = N_k(t)\delta[x - x_k(t)] \tag{8}$$

where $N_k(t)$ and $x_k(t)$ denote the electronic population and nuclear position of the kth orbit at time t, respectively. $N_k(x, t)$ can be regarded as a classical representation of the quantum-mechanical projector $\hat{P}_2(x)$, which was used in eq 2 to define the ET probability distribution $P_2(x, t)$ of the ET system. Hence the corresponding classical distribution $P_2{}^C(x, t)$ is obtained by averaging $N_k(x, t)$ over an initial phase−space density function $\rho_k = \rho_0(x_k, p_k, X_k, P_k)$ that mimics the initial state $|\Psi(0)\rangle$ of the quantum system. Summing up all POs that contribute to the ET dynamics, we get[6]

$$P_2{}^C(x, t) = \sum_k w_k \int_0^{T_k} \mathrm{d}\tau \rho_k(\tau) N_k(x, t + \tau) \tag{9}$$

where w_k and T_k denote the weight and the period of the kth orbit, respectively.

Adopting a quasiclassical approximation, moreover, the transient stimulated-emission spectrum (eq 3) can be written as average over the ET probability distribution $P_2{}^C(x, t)$, yielding[18]

$$I^C(\omega_P, \Delta t) = \int_{-\infty}^{\infty} \mathrm{d}x \int_{-\infty}^{\infty} \mathrm{d}t\, P_2{}^C(x, t) F(t)$$

$$F(t) = |\mu_{02}\epsilon_0|^2 \exp\{-(t - \Delta t)^2/\alpha^2\} \times \exp\{-[\omega_P - \Delta V(t)]^2\alpha^2\} \tag{10}$$

Due to the resonance condition $\omega_P = \Delta V(t) \equiv V_2[x(t)] - V_0[x(t)]$, the spectral evolution of the spectrum follows the wave packet motion along the coordinate x.

We are now in a position to analyze nonadiabatic quantum dynamics in terms of classical POs. Let us begin with the simplest version of the theory, that is, the approximation of $P_2(x, t)$ by a *single* orbit. Figures 2F and 2E show the classical ET probability distribution associated with the orbits A and B, respectively. The population probabilities of both orbits are seen to oscillate along the nuclear coordinate x in a similar way but with different amplitudes and periods. Furthermore, it is noticed that the ET dynamics differs for the two POs. For example, it is seen that orbit B affects a recurrence of the population probability at the left-hand-side turning points while orbit A does not. Both single-orbit contributions resemble the quantum-mechanical time evolution shown in panel A, but do not account for the details.

In a next step, we take into account the energy distribution of the initial state and consider the energy-averaged probability distribution of both orbits.[19] Figures 2D and 2C show the resulting ET probability distribution obtained for orbits A and B, respectively. As may be expected, the averaging results in an increase of the energetically accessible phase space and therefore also of the width of the probability distribution. As a consequence of the energy-dependent periods of the orbits, moreover, the peaks at the right-hand-side turning points become more pronounced and are shifted toward earlier times in the case of orbit A.

Adding the energy-averaged contributions of orbits A and B (Figure 2B), we may now analyze the quantum-mechanical ET dynamics (Figure 2A). Taking into account that only two classical orbits enter the calculation, the overall agreement and the amount of details of the classical result are remarkable. Considering the right-hand-side turning points of the quantum-mechanical probability distribution, for example, it turns out that the single peak at the first and the double peak at the second turning point can directly be explained by the superposition of the two POs. Furthermore, the weaker maxima associated with the left turning points and the intermediate area of low probability density around $x \approx 2.5$ arise as consequences of this superposition. While the classical probability distribution exhibits a clear cut-off around the turning points, the quantum distribution is more delocalized in these regions, because quantum mechanics can also invade classically forbidden regions. The limits of the two-orbit approximation can be seen at times ≈160 fs, where the quantum wave packet splits up in three components. This interference effect cannot be reproduced by a simple quasiclassical approximation.

Let us finally investigate to what extent these results transfer to the analysis of ET femtosecond spectra. Evaluating eq 10 by a sum over the two shortest POs, Figure 3 compares the quantum-mechanical spectra obtained for 10 and 20 fs probe pulses (panels A,B) to the corresponding classical results. Although the accurate reproduction of the recurrences around

the turning points deteriorates due to the field-matter interaction, the PO approximation is still in good overall agreement with the quantum data. It is interesting to note that the PO results with (panels C, D) and without (panels E, F) averaging over the energy distribution of the initial state look quite similar. This finding is explained by the fact that the spectrum is already averaged over the energy distribution of the laser field. In general, it may be noted that the averaging due to the field-matter interaction tends to support the classical approximation in that it is sufficient to include only the orbits with mean energy. Furthermore, the averaging removes the subtle interferences of the wave function at larger times, which are not amenable to a simple classical description.

To summarize, we have introduced a new theoretical concept to analyze coherent ET dynamics as monitored in femtosecond experiments. The theory combines (i) a mapping formulation, which allows us to introduce classical periodic orbits that describe nuclear motion on several coupled potential-energy surfaces and (ii) the ideas of semiclassical PO theory, which enables us to interpret complex spectra in terms of a few classical trajectories.

Considering multidimensional molecular dynamics, it may be difficult to determine the exact POs of the system. Nevertheless, recent studies on nonadiabatic photoisomerization reactions have indicated that in many cases the general concept still holds, i.e., the classical analysis allows us to obtain a classification of various types of vibronic trajectories, thereby providing an intuitive picture of nonadiabatic processes.

Acknowledgment. We thank Birgit Balzer, Bernhard Mehlig, and Michael Thoss for inspiring and helpful discussions. This work has been supported by the Deutsche Forschungsgemeinschaft and the Fonds der Chemischen Industrie.

References and Notes

(1) Zewail, A. H. Nobel Lecture, *J. Phys. Chem. A* **2000**, *104*, 5660.

(2) Michl, J.; Bonačić-Koutecký, V. *Electronic Aspects of Organic Photochemistry;* Wiley: New York, 1990. Bernardi, F.; Olivucci, M.; Robb, M. A. *Chem. Soc. Rev.* **1996**, *25*, 321. Domcke, W.; Stock, G. *Adv. Chem. Phys.* **1997**, *100*, 1.

(3) While this is well understood for small molecules (e.g., for the predissociation of NaI [ref 1]), the interpretation of coherent transients in femtosecond experiments of large systems (e.g., the photoreaction center[4]) is still under discussion. See also the special issue on *Coherences in Chemical Dynamics*; Ruhman, S., Scherer, N., Eds.; *Chem. Phys.* **1998**, *233*.

(4) Vos, M. H.; Rappaport, F.; Lambry, J.-C.; Breton, J.; Martin, J.-L. *Nature (London)* **1993**, *363*, 320. Spörlein, S.; Zinth, W.; Wachtveitl, J. *J. Phys. Chem. B* **1998**, *102*, 7492.

(5) Stock, G.; Thoss, M. *Phys. Rev. Lett.* **1997**, *78*, 578. Thoss, M.; Stock, G. *Phys. Rev. A* **1999**, *59*, 64.

(6) Dilthey, S.; Stock, G. *Phys. Rev. Lett.* **2001**, *87*, 140404. Dilthey, S.; Mehlig, B.; Stock, G. *J. Chem. Phys.* **2002**, *116*, 69.

(7) Gutzwiller, M. C. *Chaos in Classical and Quantum Mechanics;* Springer: New York, 1990. Heller, E. J. *Chaos and Quantum Physics;* North-Holland: Amsterdam, 1991. Gomez Llorente, J. M.; Pollak, E. *Annu. Rev. Phys. Chem.* **1992**, *43*, 91. Eckhardt, B. In *Periodic Orbit Theory*; Casati, G., Guarneri, I., Smilansky, U., Eds.; North-Holland: Amsterdam, 1993.

(8) Johnson, B. R.; Kinsey, J. L. *Phys. Rev. Lett.* **1989**, *62*, 1607. Jacobson, M. P.; Jung, C.; Taylor, H. S.; Field, R. W. *J. Chem. Phys.* **1999**, *111*, 600.

(9) Marcus, R. A.; Sutin, N. *Biochim. Biophys. Acta* **1985**, *811*, 265. Jortner, J., Bixon, M., Eds. *Electron Transfer: From Isolated Molecules to Biomolecules*, Adv. Chem. Phys. Vols. 106−107; Wiley: New York, 1999.

(10) The parameters of the coupled two-state system are $g = 0.05$ eV, $\omega = g$, $\kappa_2 = -\kappa_1 \equiv \kappa = 0.5g$, and $E_1 = E_2 = 0$. The uncoupled electronic ground state $|\psi_0\rangle$ is characterized by $\kappa_0 = -x_0\omega = -0.15$ eV and $E_0 = -1.775$ eV. The laser field $E_P(t) = \epsilon_0\, e^{-(t-\Delta t)^2/\alpha^2}\, e^{-i\omega_P(t-\Delta t)}$, ($\alpha^2 = \tau^2/(8 \ln 2)$) is assumed to couple only the states $|\psi_0\rangle$ and $|\psi_2\rangle$, i.e., $\hat{\mu} = |\psi_0\rangle\mu_{02}\langle\psi_2| + h.c.$, while the electronic state $|\psi_1\rangle$ is dark in absorption and emission.

(11) Experimentally, the transient emission can be discriminated from other contributions by up-conversion techniques or by using polarized laser fields.

(12) Mukamel, S. *Principles of Nonlinear Optical Spectroscopy*; University Press: Oxford, 1995.

(13) Berne, B. J., Ciccotti, G., Coker, D. F., Eds. *Quantum and Classical Dynamics in Condensed Phase Simulations*; World Scientific: Singapore, 1998.

(14) The mapping of the operators in eq 4 preserves the commutation relations and leads to an exact identity of the electronic matrix elements of the propagator.[5] In the case of a two-level system, the formalism is equivalent to Schwinger's formulation of angular momentum (see, e.g., Sakurai J. J. *Modern Quantum Mechanics*; Addison-Wesley: New York, 1994; p. 217).

(15) Meyer, H.-D.; Miller, W. H. *J. Chem. Phys.* **1979**, *70*, 3214.

(16) Thoss, M.; Miller, W. H.; Stock, G. *J. Chem. Phys.* **2000**, *112*, 10282.

(17) This can be done by setting $X^2 + P^2 = X_2^2 + P_2^2 = 1 - X_1^2 - P_1^2$. [5,15]

(18) Li, Z.; Fang, J.-Y.; Martens, C. C. *J. Chem. Phys.* **1996**, *104*, 6919. Dietz, H.; Engel, V. *J. Phys. Chem. A* **1998**, *102*, 7406. Shen, Y.-C.; Cina, J. A. *J. Chem. Phys.* **1999**, *110*, 9793.

(19) The energy distribution $w(E_i)$ of the Gaussian initial state was sampled using a step size of 0.03 eV. For each energy, the POs A and B were determined. The energy-averaged ET probability distribution is then obtained as $P_2^C = \sum_i w(E_i)P_2^C(E_i)$.